Nanoscale Topography Influences Polymer Surface Diffusion

Dapeng Wang, Chunlin He, Mark P. Stoykovich, and Daniel K. Schwartz*

Department of Chemical and Biological Engineering, University of Colorado Boulder, Boulder, Colorado 80309, United States

ABSTRACT Using high-throughput single-molecule tracking, we studied the diffusion of poly(ethylene glycol) chains at the interface between water and a hydrophobic surface patterned with an array of hexagonally arranged nanopillars. Polymer molecules displayed anomalous diffusion; in particular, they exhibited intermittent motion (*i.e.*, immobilization and "hopping") suggestive of continuous-time random walk (CTRW) behavior associated with desorption-mediated surface diffusion. The statistics of the molecular trajectories changed systematically on surfaces with pillars of increasing height, exhibiting motion that was increasingly subdiffusive and with longer waiting times between diffusive steps. The trajectories were well-described by kinetic Monte Carlo simulations of CTRW motion in the presence of randomly distributed permeable obstacles, where the permeability (the main undetermined parameter) was conceptually related to the obstacle height. These findings provide new insights into the mechanisms of interfacial transport in the presence of obstacles and on nanotopographically patterned surfaces.

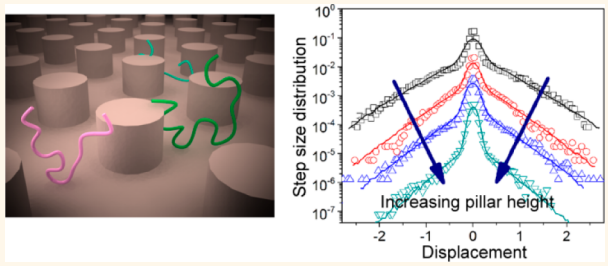

KEYWORDS: single-molecule fluorescence imaging · polymer · surface diffusion · obstructed diffusion · CTRW

The diffusion of polymers on solid surfaces has broad implications in diverse chemical processes, including surface-based biosensors,[1] polymer separations,[2] lubrication,[3] heterogeneous catalysis,[4] surface-mediated supermolecular self-assembly,[5] *etc.* Moreover, surface transport, and its underlying mechanisms, greatly influences the efficiency of chemical processes that rely on molecular searching for surface targets.[6] While polymer surface diffusion has been intensively explored in the past decade,[7−17] there is little understanding of the impact of surface heterogeneity on surface transport mechanisms.

The traditional view of polymer surface diffusion is based on a picture of adsorbing flexible chains, in which a chain adsorbs at a liquid−solid interface due to noncovalent interactions between polymer segments and the particular surface chemistry.[18−20] In this context, the binding energy of each segment of a poly(ethyelene glycol) (PEG) chain to a hydrophobic surface is estimated to be 0.5−1 k_BT.[7] In this picture, the adsorbed polymers eventually adopt an equilibrium distribution of surface conformations, traditionally labeled "loop-train-tail" conformations, and are expected to exhibit surface diffusion based on reptation and transitions within this ensemble of conformations. However, it has been recently demonstrated in two independent laboratories that polymers, in fact, exhibit intermittent hopping at the liquid−solid interface.[17,21,22] The details of this motion are inconsistent with the conventional view of 2D diffusion of adsorbed flexible chains, but are in line with the observations of long flights for adsorbed small molecules on a solid surface.[23−25] The intermittent motion of polymers, small molecules, and biomolecules has been successfully described as a continuous-time random walk process (CTRW).[26−28] A proposed mechanism for this behavior is that the hopping is a desorption-mediated process where a polymer chain desorbs from the surface, diffuses through the bulk liquid, and finally reattaches at a new location.[16,21,22,29,30] In this picture, the height, density, and connectivity of surface nanostructures would potentially have a significant influence. For example, corners and edges could serve as sites where polymers are entropically stabilized, and high-points on the surface could serve as obstacles to interrupt some three-dimensional flights. The experiments

* Address correspondence to daniel.schwartz@colorado.edu.

Received for review November 7, 2014 and accepted January 23, 2015.

Published online January 24, 2015
10.1021/nn506376n

described here are designed to test these hypotheses.

While the influence of roughness on surface diffusion has been recognized,[31] the detailed role of surface topography on the surface transport remains largely unexplored due to the lack of precise control of topography on nanometer length scales. Several approaches are available to fabricate nanometer-scale surface structures, including high-resolution lithographic methods such as electron-beam and interference lithography,[32] ion beam milling and multiphoton adsorption polymerization.[33] Here, we employed an approach known as block copolymer lithography,[34] which is based on the self-assembly of periodic structures in thin films of diblock copolymers comprised of two immiscible polymer blocks.[35] Advantageously, block copolymer lithography enables high-throughput fabrication of periodic nanostructures with tunable dimensions in the range of 5−100 nm.[36−39] In particular, polystyrene-*b*-poly(methyl methacrylate) (PS-*b*-PMMA), thin films with varying PS fractions have been observed to form various periodic microdomains, including hexagonally arranged spots or periodic lines after thermal or solvent annealing.[40−42]

The use of block polymer lithography allowed us to study the role of well-defined surface topography on polymer surface diffusion by systematically varying the height of the surface nanostructures. In particular, we studied PEG chains (M_W = 40 kg/mol) on a surface patterned by hexagonally arranged pillars with heights in the range of 3−7 nm. The selected molecular weight ensured a flexible polymer chain because the radius of gyration (1.5 times larger than the hydrodynamic radius in a θ-condition,[19] ∼ 7.5 nm for PEG with M_W = 40 kg/mol) is much greater than the persistence length of PEG (∼0.3 nm).[43] Using high-throughput single-molecule tracking, we found that polymer motion exhibited intermittent hopping on the pillar-patterned surfaces where the waiting times between hops and the step-sizes associated with hopping events were systematically influenced by the pillar heights. The details of the molecular trajectories were well-described by simulations using a continuous-time random walk (CTRW) model obstructed by randomly distributed semipermeable obstacles. Consistent with expectations for desorption-mediated diffusion, the trajectories of polymers were influenced more strongly by taller obstacles.

RESULTS AND DISCUSSIONS

Surface Nanostructures. Following a previously described approach,[44] we fabricated an array of silica nanopillars using PS-*b*-PMMA thin films as a template. Figure 1a shows a schematic representation of the fabrication process. PS-*b*-PMMA solution was spin-coated on a fused-silica surface functionalized with a random copolymer of PS-*r*-PMMA with a monomer ratio of 64:36 (PS:PMMA). The thin film of block

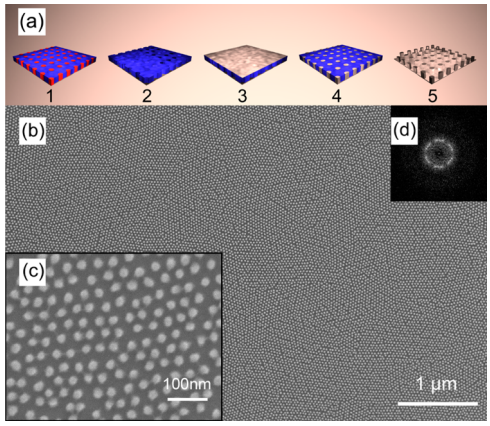

Figure 1. (a) Schematic view of the preparation procedure for an array of silica pillars. (1) Self-assembly of PS-*b*-PMMA thin films. The blue and red indicate the PS and PMMA blocks, respectively. (2) PMMA domains are removed from the thin film. (3) Spin-coating of PDMS solutions onto the PS template films. (4) PDMS diffuses into the nanopores. (5) Silica pillars are formed after oxygen plasma treatment. (b) A representative SEM image of an array of silica pillars patterned on the surface. (c) A magnified image of a smaller area of the pillar array. (d) A fast Fourier transform of a portion of (b).

copolymers self-assembled upon thermal annealing, exhibiting an array of PMMA cylindrical microdomains oriented normal to the surface (Figure 1a-1). The PMMA blocks were then removed using UV irradiation and washing by acetic acid (a good solvent for PMMA but a nonsolvent for PS), and the remaining PS template was processed with an oxygen-plasma to further remove any remaining PMMA (Figure 1a-2). The nanostructured template after PMMA removal is shown in Supporting Information Figure S1 where a hexagonal array of nanopores was observed. Linear polydimethylsiloxane (PDMS) solution was then spin-coated onto these PS template films (Figure 1a-3) and vacuum-annealed at 80 °C to allow the PDMS to diffuse into the nanopores (Figure 1a-4). This annealing temperature was well below the glass transition temperature of PS. The organic materials on surface were then totally degraded by an oxygen-plasma treatment, while transforming the PDMS in the nanopores into silica (Figure 1a-5). An additional etch in CF_4 plasma was used to remove any remaining traces of PDMS.

Figure 1b,c shows images of a representative patterned surface observed by scanning electron microcopy (SEM). The average diameter of the pillars, determined using quantitative image analysis (ImageJ), was 24 nm. Figure 1d shows a fast Fourier transform (FFT) of a small area of Figure 1b and exhibits sets of six symmetrical hexagonally arranged spots, corresponding to a two-dimensional hexagonal lattice with a regular lattice spacing of 37 nm. The presence of three distinct sets of spots in the FFT is indicative of polycrystallinity in the patterned features over large areas, in this case with three grains of different orientation being observed.

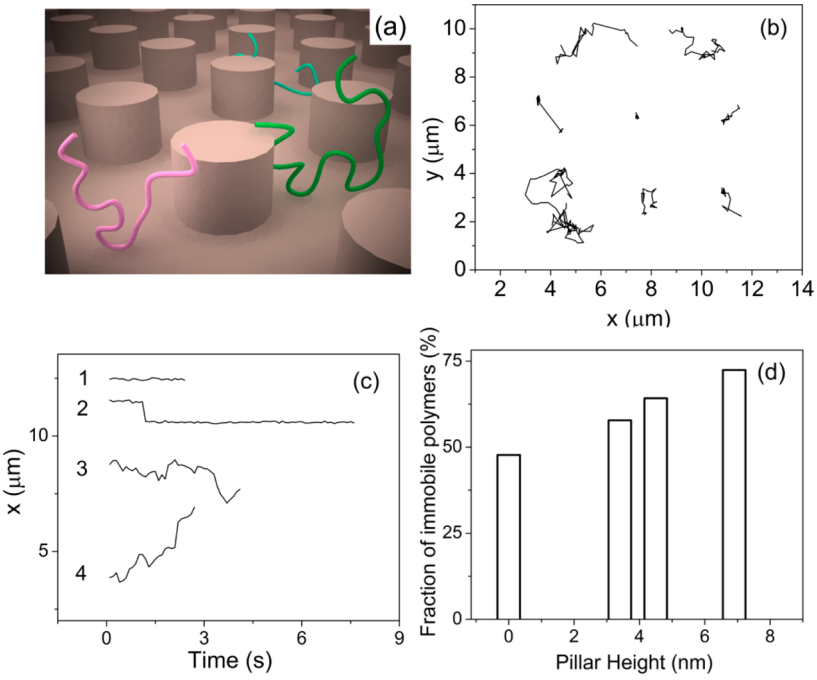

Figure 2. (a) Cartoon of polymer chains (colorful coils) adsorbed on a pillar patterned surface. (b) Representative trajectories of PEG on a patterned surface. (c) Representative trajectories showing the lateral position of PEG as a function of time. (d) Fraction of immobile polymers as a function of the pillar height.

The height of the pillars was controlled by using PDMS solutions with different concentrations. Ellipsometry measurements were used to determine the pillar height, yielding values of 3.4, 4.5, and 6.9 nm. Finally, the patterned surfaces were functionalized with a hydrophobic monolayer of tetramethylsilane (TMS). The experimental methods are detailed in the Experimental Details section.

Single-Molecule Trajectories. Total internal reflection fluorescence microscopy was used to track the motion of individual polymer chains at the interface between the water and either flat or pillar patterned surfaces (Figure 2a). All surfaces were hydrophobically modified with a trimethylsilane monolayer. Because the pillars and the underlying substrate were both comprised of silica, both the substrate and pillars were modified by trimethylsilane and were nominally identical in terms of their chemical interactions with PEG. Because of their fast mobility in the bulk water phase, unadsorbed polymer molecules were blurred, and the dynamics of polymer chains were resolved only for molecules adsorbed at the interface. The center-of-intensity positions of nearest-neighbor objects in consecutive images were connected to construct molecular trajectories as described previously.[45] Approximately 800−1000 trajectories (with a surface residence time longer than 1 s) were accumulated for each type of surface. A typical set of trajectories is shown in Figure 1b. We observed significant heterogeneity between trajectories of individual molecules. The trajectories could be categorized into two distinct classes: more than 50% were immobile during their entire period of adsorption (**1** in Figure 2c), while the remainder exhibited intermittent hopping in which the polymer jumped from spot to spot with a distribution of waiting times. Trajectories often contained multiple hops, which occasionally spanned distances over 1 μm (**3**, **4** in Figure 2c). We identified immobile molecules by measuring the distance between the first and the last position; a threshold of 0.2 μm was used to define immobility. As illustrated in Figure 2d, the fraction of immobile polymers increased systematically as the pillar height increased. A further increase of the pillar height resulted in essentially complete immobilization of PEG on the surface. This scenario was ascribed to the enhanced interaction between the surface and PEG chains due to increased surface area. This finding was robust with respect to variations in the threshold. For example, changing the distance threshold used to define immobilization by $\pm$0.04 μm resulted in a $\pm$ 7% change in the fraction of immobile polymers and negligible change in the approximate power-law exponent in the waiting time distribution. The fact that the presence of nanostructured topography significantly increased the fraction of immobile polymers is not to say that they are necessarily completely immobile, but they certainly exhibited long waiting times, suggestive of an increased number of strong binding sites, perhaps at sites of high negative surface curvature (*e.g.*, corners).

To quantify the polymer motion, we first calculated the ensemble-average mean squared displacement (MSD), according to $\langle \Delta \mathbf{r}(\tau)^2 \rangle = \langle |\mathbf{r}(t+\tau) - \mathbf{r}(t)|^2 \rangle$, where $\mathbf{r}$ is the position in the x−y plane and τ is the time

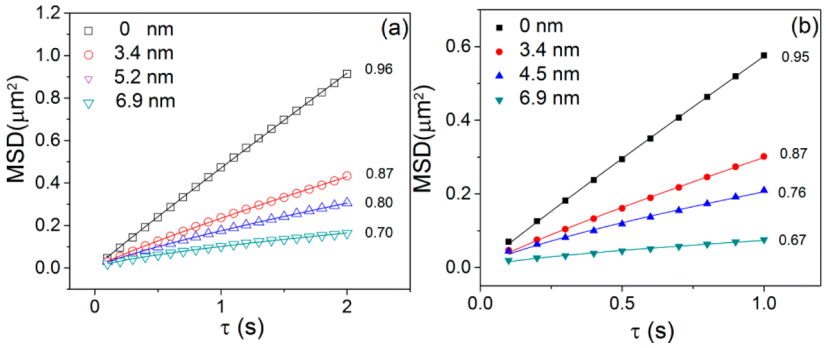

Figure 3. Mean squared displacement *versus* time interval. Symbols represent data from (a) experiments for PEG on either flat (0 nm) or pillar-patterned surfaces, or (b) Monte Carlo simulations using the parameters shown in Supporting Information Table S1. In all cases, the solid lines represent power-law fits to the form MSD = $4D\tau^{\xi}$. The best-fit exponents are annotated at right.

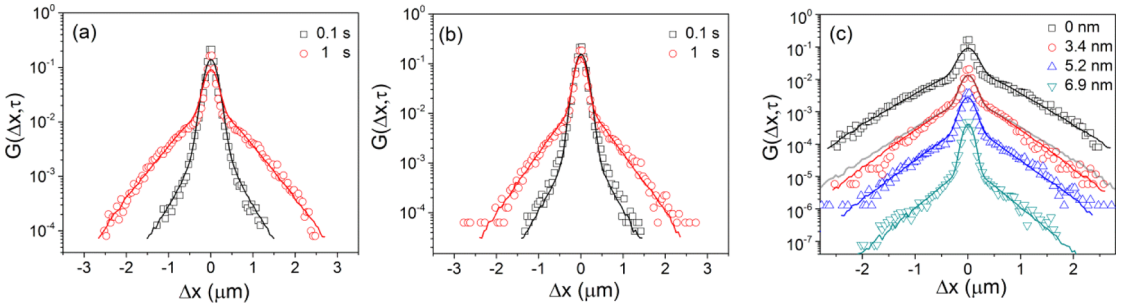

Figure 4. Step-size distribution of PEG on a (a) flat surface and (b) surface patterned with topography of 4.5 nm in height at τ = 0.1 and 1 s. (c) Step-size distribution of PEG on flat and pillar patterned surfaces at τ = 1 s. The symbols denote the experimental data, and the solid lines indicate the simulation results using the models described in the main text. The parameters in the simulation were listed in Supporting Information Table S1. The gray line in (c) represents the result of a simulation with completely permeable obstacles as described in the text. The curves in (c) were shifted downward by factors of 1/9, 1/50, and 1/500 for PEG on the surfaces with 3.4, 4.5, and 6.9 nm topography, respectively.

interval. The brackets denote averaging performed over all trajectories. Figure 3a shows plots of MSD *vs* τ for PEG on all surfaces studied. For PEG chains on the flat TMS-coated silica surface, the MSD increased approximately linearly with τ (Figure 3a) as expected for Fickian diffusion, consistent with previous observations of a similar system.[17,21] However, we observed that the MSDs became systematically smaller as the pillar height increased. The MSD data were fitted using the power law relation MSD = $4D\tau^{\xi}$, and exhibited systemically smaller exponents with increasing pillar height. In particular, the exponent decreased from 0.87 for 3.4 nm pillars to approximately 0.70 for 6.9 nm pillars, suggesting an increasingly subdiffusive process.

To further quantify the lateral diffusion, we calculated the ensemble-averaged step-size distribution $G(r, \tau)$ as described previously.[46] Figure 4a,b shows $G(r, \tau)$ for PEG on a flat surface and a patterned 4.5 nm pillar surface. Qualitatively, the shapes of $G(r, \tau)$ on flat and patterned surfaces were similar and could be divided into two parts: a narrow central peak and extended tails.

The central peaks for all surfaces were invariant as a function of τ, and could be described by a Gaussian $G(r, \tau) \sim \exp[-\Delta x^2/2\sigma^2]$, yielding a width $\sigma \approx 0.08\ \mu$m due to imperfect localization precision (both static and dynamic). Motions smaller than this limit during periods of immobilization were not resolvable. Therefore, the possible slow diffusion described by *in situ* TEM/AFM methods was treated as immobility.[47−50] As shown in Figure 3c, the magnitude of the central peaks increased qualitatively for surfaces with taller pillars, consistent with the increasing fraction of immobile polymers (Figure 2d). This evolution of the central peak for different surfaces made a significant contribution to the observed trends of the ensemble averaged MSD illustrated in Figure 3a; *i.e.*, some of the apparent subdiffusive behavior was due to an increasing immobile fraction of steps for surfaces with higher pillars.

We also found that the mobile fraction of steps exhibited subdiffusive behavior on the pillar-patterned surfaces. To see this clearly, we normalized $G(r,\tau)$ (calculated for different values of τ) by the factor $x_{norm} = r/\tau^{0.5}$ to account for the dependence of $r \sim \tau^{0.5}$ expected for Fickian diffusion. As expected, we found that the tails of the normalized $G(r,\tau)$ at different τ were similar to those for PEG on flat surfaces (Supporting Information Figure S3a), again consistent with approximate Fickian diffusion during hopping. However, the tails of the normalized $G(r,\tau)$ for PEG on patterned surface did not collapse onto a master curve (Supporting Information Figure S3b), demonstrating that

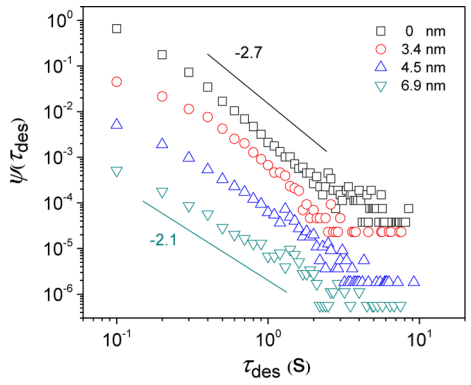

Figure 5. Distribution of waiting times between intermittent hopping events. Symbols denote the experimental data for PEG on flat and topographically patterned surfaces after removing trajectories of the immobile polymers. Curves for data on 3.4, 4.5, and 6.9 nm topographically patterned surfaces are shifted downward by factors of 1/10, 1/100, and 1/1000, respectively. The solid lines show approximate power law exponents, $-(1 + \alpha)$, for flat and 6.9 nm patterned surfaces, as annotated.

the hopping motion itself was subdiffusive on the pillar-patterned surfaces.

The overall shape of $G(r,\tau)$ depended on the value of τ. For short time intervals (*e.g.* τ = 0.1 s), the distributions were heavy-tailed, decaying more slowly than a Gaussian distribution. Interestingly, for larger time intervals (*e.g.* τ = 1s), the tails of $G(r,\tau$ = 1s) reverted to an approximate Gaussian (Supporting Information Figure S2 and Figure 4) form, consistent with expectations from the central limit theorem. Qualitatively, we observed decreased step-size statistics with increasing pillar height (Figure 4c).

The intermittent hopping was further evaluated by calculating the waiting-time intervals, τ_{des}, between two consecutive hops in a trajectory. The threshold distance used to distinguish hops from immobilization was defined as 0.2 um, consistent with the parameters that were used to define the fraction of immobile polymers. Figure 5 shows the waiting-time distributions of PEG on both flat and patterned surfaces after removing the immobile polymers of trajectories. For all samples studied, the distribution could be characterized by approximate power-law behavior $\psi(\tau_{des}) \sim {\tau_{des}}^{-(1+\alpha)}$ with α decreasing systematically from 1.7 to 1.1. In the case of a single binding energy barrier, the waiting time distribution would be a decaying exponential. The observed power-law distribution, therefore, suggested a spectrum of binding energies, as was also observed in previous work with a variety of molecular species.[22] Interestingly, on the pillar-patterned surfaces, the power-law parameter α in the relation $\psi(\tau_{des}) \sim {\tau_{des}}^{-(1+\alpha)}$ decreased with increasing pillar height suggesting that the increased surface area, and/or increased area of curved surface, associated with the topographically patterned surfaces may have facilitated strong binding with a wide variety of polymer configurations.

It is important to note that while the waiting time distributions and the fundamental step-size distribution (as discussed further below) exhibited approximate power-law behavior within experimentally accessible time and length scales, these are only approximate expressions and do not necessarily reflect the behavior at extreme values. Presumably, the deviation from power law behavior at shorter/longer time and length scales results in well-behaved distributions that satisfy the central limit theorem (*i.e.*, they have well-defined first and second moments).

Taken together, the experimental observations described above clearly indicated that the pillar-patterned surfaces influenced the polymer motion in several ways. In particular, they systematically decreased the polymer surface mobility with increasing pillar height, specifically resulting in an enhanced fraction of immobile species, a broader distribution of waiting times, increasingly subdiffusive MSD curves, and a narrowing of the non-Gaussian step-size distributions.

CTRW Simulations with Obstructions. In previous work, the intermittent hopping of molecules on surfaces was successfully modeled as a continuous time random walk (CTRW) using power-law step-size (approximating the predictions of analytical theory) and waiting-time (based on empirical observations) distributions.[21] The CTRW model is typically used to describe stochastic switches between immobilization and mobilization with given distributions of jump lengths and waiting times. Due to the topographic complexity of the patterned surfaces, a standard CTRW model was not sufficient to describe the polymer diffusion on such surfaces. Therefore, we hypothesized that a CTRW incorporating obstacles could potentially describe the statistics of the trajectories observed here and provide insight into the mechanistic role of the topographical heterogeneity. We chose to model the height of pillars by incorporating semipermeable obstacles, with the idea that a taller pillar would have a greater chance of interrupting a given molecular "hop" than a shorter pillar. The computational details of the CTRW simulations with obstructions can be found in the Experimental Details section. It should be noted that in the simulations, a PEG molecule can adsorb on both the pillars and substrate, but obstruction can take place only when a diffusion molecule attempts to move to a lattice site that is occupied by a pillar.

The parameters used in the simulations were designed to be as similar as possible to the associated experimentally measured values. For example, we placed randomly distributed obstacles on the simulated "surface" with an areal coverage of 32.6% because the volume fraction of PMMA in the PMMA-*b*-PS block copolymer thin film (the template) was approximately 30% and the areal coverage of the pillar array was determined to be 32.6% using direct image

analysis of electron micrographs. Also, the molecules were divided randomly into two groups, immobile polymers and mobile polymers, based on the experimentally measured immobile and mobile population fractions (Figure 2d). The immobile polymers were fixed at the same lattice site for a given lifetime. To model the mobile polymers, we simulated two-dimensional CTRW dynamics using power law functions for the waiting-time distribution $\psi(\tau_{des}) \sim \tau_{des}^{-(1+\alpha)}$ and the step-size distribution $f(r) \sim r^{-\beta}$ based on our experimental observations. The values of parameters used in the simulations are listed in Table S1 in the Supporting Information. In the simulations, the parameter P, which determined the permeability of the obstacles, was the most significant undetermined parameter.

Comparison between Experiments and Simulations. The CTRW simulations with obstructions were compared with the experimental observations. As mentioned above, four main features, the step-size distribution $f(r)$, the waiting time distribution $\psi(\tau_{des})$, the fraction of immobile species F, and the permeability parameter P were required to model the surface diffusion in CTRW simulations. The parameters associated with the step-size distribution $f(r)$, the waiting time distribution $\psi(\tau_{des})$, and the fraction of immobile species F were chosen to be similar to the experimentally measured values, leaving the parameter P (conceptually related to pillar height) as the only undetermined parameter in the simulations. By systematically increasing P from 0 (on the flat surface) to 0.5 (on the 6.9 nm patterned surface), the simulations successfully represented the experimental step-size distributions at different values of τ (Figure 4a,b), or at the same value of τ on patterned surfaces with different pillar heights (Figure 4c). The values of P that best described our data were 0, 0.30, 0.35, and 0.50 for d = 0, 3.4, 4.5, 6.9 nm, respectively. This suggested that 3.4 nm pillars have a 30% probability to block a flight encountering the obstacle, while the blocking efficiency increased to 35% and 50% for the 4.5 and 6.9 nm pillars, respectively.

We also compared the simulation results with experimental MSD measurements. Using the same parameters that gave satisfactory agreement with step-size distributions, the plots of simulated MSD against τ are shown in Figure 3b, where the scaling parameters ξ of the simulated MSD data *versus* τ were in excellent agreement with the experimental results on various patterned surfaces (Figure 3). In particular, the simulations for obstacles that were increasingly efficient at blocking trajectories became increasingly subdiffusive, as was also observed experimentally for taller pillars.

To test the sensitivity of this analysis, we kept $P = 0$ (*i.e.*, completely permeable obstacles) while adjusting the parameter β in the step size distribution, $f(r)$, and the immobile fraction, F, to fit the data. However, manipulating these two parameters failed to provide good agreement with data in all cases, *i.e.*, the simulations were not consistent with the scaling of the MSD data and the behavior of $G(\Delta x,\tau)$ at different τ. Likewise, if we kept $P = 0$, systematic changes to the parameter α in the waiting time distribution, $\psi(\tau_{des})$, and the immobile fraction F did not produce satisfactory fits for PEG on the various surfaces. An example is shown in Figure 4c (the gray line) for a simple CTRW simulation with permeable obstacles ($P = 0$), that used parameters appropriate for PEG on the surface with 3.4 nm pillars. Importantly, this indicated that the observed subdiffusive behavior could not be described simply by changing the waiting time distribution and immobile fraction. Taken together, these tests indicated that it is vital to include obstructed diffusion to achieve consistency between simulations and experiments.

Microscopic Interpretation. The observations presented above suggest that pillars influenced the dynamics of polymer surface transport in three significant ways: the immobilized fraction was increased, the distribution of waiting times broadened, and flights were obstructed. In the first and second cases, these conclusions were based on clear empirical evidence, *e.g.*, the increase of the immobilized fraction shown in Figure 2d and the broadening of the waiting time distributions shown in Figure 5. Both of these phenomena occurred on time scales that were directly accessible, and were likely related to the existence of strong binding sites and/or a greater number of strongly bound conformational states (entropic stabilization) in the vicinity of the pillars. As described above, the heavy-tailed nature of the waiting-time distribution, suggested the presence of a broad spectrum of binding energies, possibly related to sequential and independent desorption of individual segments. In previous work, we carefully studied the dependence of the waiting time distribution (and mean waiting time) on molecular weight on "flat" hydrophobic surfaces, and observed scaling behavior that was consistent with "3D coil" molecular conformations, as opposed to pancakes, suggesting that molecular relaxation to flattened conformations was slow compared to the typical desorption rate.[21]

As demonstrated above, however, the increased immobile fraction and lengthened waiting-time distributions were not sufficient to describe the observed phenomena, including the subdiffusive nature of the mean squared displacement and the narrowing of the step-size distribution. Therefore, we attempted to describe these additional effects of the pillars in the context of desorption-mediated interfacial diffusion.[26,51] In this theory, adsorbate molecules detach from an interface and execute three-dimensional "flights", re-encountering the interface with a distribution of first-return times. Most of the return times are

very short; however, since the readsorption probability is not unity, most molecules execute multiple hops prior to readsorption. These flights, and their potential obstruction, occur on time scales that are not experimentally accessible. For example, using results from a previous study,[7] we can estimate a fundamental time scale associated with the Brownian motion of a 40 kg/mol PEG molecule in the aqueous phase, *e.g.*, the time required to diffuse a distance equivalent to the molecular size, or to the characteristic size of surface features. Such a calculation results in time scales on the order of $\sim$1 μs, which is many orders of magnitude shorter than the temporal resolution of our experiments. Because of this discrepancy in time scales, we used kinetic Monte Carlo simulations to explore the influence of obstacles on such flights. In particular, it has been shown that obstructed diffusion can result in decreased diffusivity[52−54] and anomalous diffusion.[55−58]

The simulations were based within the framework of CTRW phenomena, where a waiting time distribution and a flight-length distribution are required to describe motion.[21,22] The distributions used were simplified power law distributions based on empirical observations, with no undetermined parameters. Semipermeable obstacles were placed randomly at the experimentally measured density, and the effect of obstacle permeability was explored. We found that by systematically decreasing the obstacle permeability, the mean squared displacement became increasingly subdiffusive, and the step size distribution (at a given time interval) became narrower. The same trends were observed experimentally for obstacles of increasing height. Notably, we identified particular values of the permeability parameter P that provided excellent agreement with all aspects of the measured data (which could not be explained in the absence of the obstacles). Interestingly, the data for taller pillars corresponded to simulations with less permeable obstacles. This led us to envision the obstacles as serving to confine the hopping adsorbate molecules, increasing the number of surface encounters, and therefore reducing the probability of very long flights.

CONCLUSIONS

The present study addresses a fundamental question regarding how individual polymer chains diffuse on surfaces with topographic complexity. Diffusion of individual polymer chains on the pillar-patterned surface, identified by high-throughput single-molecule tracking, exhibited intermittent hopping with decreased (and subdiffusive) mobility and longer waiting times than on flat surfaces. This behavior was quantitatively modeled using simulations of CTRW motion that incorporated semipermeable obstacles.

The obstruction to surface transport created by topographic structure has significant implications for real-world molecular processes that involve surface diffusion, since the aspect ratio of surface structures (topographically patterned surfaces) is expected to impact the nature of the motion. For example, in heterogeneous catalysis, polydisperse nanoparticles are often deposited on larger inert support powders. Although the primary motivation for this catalyst structure is to increase the accessible surface area of the expensive catalyst, we suggest that catalytic activity, which depends both on the accessibility of reactive sites to reactants and the ability of products to be removed from the surface, may be highly sensitive to the detailed structure of the catalyst particles, not only their size, but also their placement.

EXPERIMENTAL DETAILS

Materials. Hexamethyldisilazane was purchased from Fisher Scientific. Block copolymer polystyrene-*b*-poly(methyl methacrylate) (PS-*b*-PMMA) was purchased from Polymer Source, Inc. (Dorval, Quebec, Canada) and used as received. The number-average molecular weights M_n of the PS and PMMA blocks were 46 and 21 kg/mol with a polydispersity index (PDI) of 1.09. The polymer chain, amino-terminated methoxy poly(ethyelene glycol) (PEG) with M_n = 40 kg/mL was reacted with fluorescein isothiocyanate (PEG, Nanocs). Our control experiments showed that fluorescein isothiocyanate did not adsorb on the surface studied, eliminating the possibility that polymers adsorb by their fluorescent tag. The PEG was dissolved in 1 mM sodium borate buffer at concentrations of 10^{-14} to 10^{-12} M, enabling the surface coverage to be lower than 0.03 molecule/μm^2. We can eliminate the likelihood for any polymer−polymer interactions at such low concentrations.

Surface Preparation. To prepare the flat surfaces, fused silica wafers were washed by a 2% Micro 90 solution and then rinsed with water. Wafers were then immersed in a 70 °C piranha solution for 4 h followed by a UV−ozone treatment for 0.5 h and were finally exposed to hexamethyldisilazane vapors for 24 h at room temperature in a vacuum desiccator to prepare a trimethylsilane (TMS) monolayer. Following deposition, wafers were rinsed with toluene and water, dried under nitrogen gas before assembly into a custom-designed flow cell for experiments.

To prepare patterned surfaces, PS-*b*-PMMA copolymer was dissolved in toluene (analytical grade, Fisher) at room temperature for 24 h to prepare a 1.5 wt % polymer solution. PS-*b*-PMMA thin films were fabricated by spin-coating at 4000 rpm for 45 s. Block copolymer films were annealed at 190 °C for 24 h in a vacuum chamber. Following thermal annealing, the PMMA was removed using UV exposure, acetic acid washing and oxygen plasma etching. Linear PDMS (4000 cSt kinematic viscosity, Aldrich) in heptane with varying concentrations in the range of 0.1−0.2 wt % was spin-coated onto the PMMA-removed films at 2000 rpm and annealed at 80 °C for 6 h under vacuum. Then, the surface was treated by oxygen plasma and a brief CF_4 plasma etch. Finally, the surfaces were exposed to hexamethyldisilazane vapors for 24 h at room temperature in a vacuum desiccator and rinsed with toluene and water before imaging.

Total Internal Reflection Fluorescence Microscopy. Experiments were performed using a Nikon TE-2000 microscope with a 60× water immersion objective outfitted with a custom-built prism-based illumination system. An EMCCD camera (model Cascade-II:512, Photometrics, Inc.) operating at −95 °C was employed to capture sequences of images with an acquisition

time of 0.1 s. A Cobalt Samba laser emitting at 491 nm was used as the excitation source for the fluorescent label. The laser was carefully oriented to produce an evanescent field at the interface between fused silica and aqueous solutions. At least 30 movies with 100 s duration were continuously captured on at least four different surface regions. The measurements were repeated on multiple days. The movies were analyzed by binning the movies into small time intervals. Within each bin the objects were identified and tracked by a custom-designed tracking algorithm.

CTRW Simulation with Obstructions. A modified 2D square lattice CTRW simulation was designed to incorporate obstacles in the following way. Each lattice site was equivalent to a $0.01 \times 0.01\ \mu$m area, and an obstacle was modeled as a square containing four lattice sites. The obstacles were randomly distributed on the lattice with an area fraction of 32.6%. The walker, a PEG chain with hydrodynamic radius $R_H \approx 5$ nm occupied a lattice site, initially chosen at random. Mimicking the experimental results, the walkers were divided randomly into two groups, immobile polymers and mobile polymers, based on the experimentally measured immobile and mobile population fractions. The immobile polymers were fixed at the same lattice site for a given lifetime and the apparent position was determined by a Gaussian distributed noise function, $\exp(-r^2/l^2)$ with $l = 0.06-0.09\ \mu$m dictated by the experimental localization precision of a given experiment. For mobile polymers, the motion of the molecules alternated between periods of immobility and mobility with an experimentally measured waiting time distribution $\psi(\tau_{des}) \sim \tau_{des}^{-(1+\alpha)}$ for $t_b < \tau_{des} < t_e$, where t_b and t_e are the upper limit and lower limit of τ_{des}. During the waiting times, the apparent molecular location was represented by a Gaussian noise function, as mentioned above. During each mobile period, a step was drawn from the step-size distribution $f(r) \sim r^{-\beta}$ with $r_b < r < r_e$, where r_b and r_e are the upper limit and lower limit of r. For the desorption-mediated hop, the distribution of step-size scales from $f(r) \sim r^{-1}$ to $f(r) \sim r^{-3}$ at small and large r, respectively. In our current work, we found that the value of $\beta = 2.1$ was a good representation to sample r over a large range of length. For each sampled step size r, the molecule executed a random walk on the square lattice with an appropriate number of steps to explore the distance r ($n = r^2/0.0001$). During the random walk, if a molecule attempted to move to an adjacent lattice site occupied by an obstacle, there was a probability, P, that the move was not accepted, and particle remained in its original place and canceled its next two steps to simulate the interaction between polymer and obstacles. Thus, P was defined to represent the probability that a given obstacle would successfully block a given step. The detailed simulation parameters are given in Supporting Information.

Ellipsometry Measurements. We employed a variable-angle spectroscopic ellipsometry (J.A. Woollam, Lincoln, NE) to estimate the thickness of patterned surface films. Oxidized silicon wafers (WRS Materials) were used as substrates for the ellipsometry measurement. The chemical properties of the native oxide of silicon wafers are expected to be similar to the fused silica. An isotropic three-interface optical model was used to fit the change in phase and amplitude of the polarized light measured at varying angles in the range of 60° to 80° with 5° for each step.

Scanning Electron Microscope. The surface structures were imaged by a JEOL JSM-7401F scanning electron microscope (SEM) operating at a 1 kV sample bias and a 2 kV accelerating voltage. The emission current used was 1 mA. To optimize the image quality, silicon wafers were used as substrates for the SEM measurements. The chemical properties of the native oxide on silicon wafers are expected to be similar to the fused silica. Moreover, the surfaces were always functionalized with a $\sim$ 5 nm layer of random copolymer PS-*r*-PMMA. Therefore, the self-assembly of PS-*b*-PMMA and the succeeding processes were expected to be insensitive to subtle differences oxides on the underlying substrate. In fact, our control experiments showed that the surface morphologies in each step of surface processing were very similar on fused silica and oxidized silicon wafers.

Conflict of Interest: The authors declare no competing financial interest.

Acknowledgment. The authors acknowledge Dr. Renfeng Hu for stimulating discussions. The authors thank the U.S. Department of Energy Basic Energy Sciences, Chemical Sciences, Geosciences, Biosciences Division (DE-SC0001854) for support of D.W. and the National Science Foundation (Award CHE-1306108) for the development of methods and instrumentation used in this research.

Supporting Information Available: Supplemental figures mentioned in the main text and the parameters used in simulation. This material is available free of charge *via* the Internet at http://pubs.acs.org.

REFERENCES AND NOTES

1. Squires, T. M.; Messinger, R. J.; Manalis, S. R. Making It Stick: Convection, Reaction and Diffusion in Surface-Based Biosensors. *Nat. Biotechnol.* **2008**, *26*, 417–426.
2. Chou, C.-F.; Bakajin, O.; Turner, S. W.; Duke, T. A.; Chan, S. S.; Cox, E. C.; Craighead, H. G.; Austin, R. H. Sorting by Diffusion: An Asymmetric Obstacle Course for Continuous Molecular Separation. *Proc. Natl. Acad. Sci. U.S.A.* **1999**, *96*, 13762–13765.
3. Urbakh, M.; Klafter, J.; Gourdon, D.; Israelachvili, J. The Nonlinear Nature of Friction. *Nature* **2004**, *430*, 525–528.
4. Kolasinski, K. K. *Surface Science: Foundations of Catalysis and Nanoscience*; John Wiley & Sons: New York, 2012.
5. van Hameren, R.; van Buul, A. M.; Castriciano, M. A.; Villari, V.; Micali, N.; Schön, P.; Speller, S.; Monsù Scolaro, L.; Rowan, A. E.; Elemans, J. A. Supramolecular Porphyrin Polymers in Solution and at the Solid-Liquid Interface. *Nano Lett.* **2008**, *8*, 253–259.
6. Soula, H.; Care, B.; Beslon, G.; Berry, H. Anomalous *versus* Slowed-Down Brownian Diffusion in the Ligand-Binding Equilibrium. *Biophys. J.* **2013**, *105*, 2064–73.
7. Sukhishvili, S. A.; Chen, Y.; Muller, J. D.; Gratton, E.; Schweizer, K. S.; Granick, S. Materials Science—Diffusion of a Polymer 'Pancake'. *Nature* **2000**, *406*, 146–146.
8. Maier, B.; Radler, J. O. DNA on Fluid Membranes: A model Polymer in Two Dimensions. *Macromolecules* **2000**, *33*, 7185–7194.
9. Sukhishvili, S. A.; Chen, Y.; Müller, J. D.; Gratton, E.; Schweizer, K. S.; Granick, S. Surface Diffusion of Poly(ethylene glycol). *Macromolecules* **2002**, *35*, 1776–1784.
10. Pu, Y.; Rafailovich, M.; Sokolov, J.; Gersappe, D.; Peterson, T.; Wu, W. L.; Schwarz, S. Mobility of Polymer Chains Confined at a Free Surface. *Phys. Rev. Lett.* **2001**, *87*, 206101.
11. Zhao, J.; Granick, S. Polymer Lateral Diffusion at the Solid-Liquid Interface. *J. Am. Chem. Soc.* **2004**, *126*, 6242–6243.
12. Qian, H.-J.; Chen, L.-J.; Lu, Z.-Y.; Li, Z.-S. Surface Diffusion Dynamics of a Single Polymer Chain in Dilute Solution. *Phys. Rev. Lett.* **2007**, *99*, 068301.
13. Desai, T.; Keblinski, P.; Kumar, S.; Granick, S. Modeling Diffusion of Adsorbed Polymer with Explicit Solvent. *Phys. Rev. Lett.* **2007**, *98*, 218301.
14. Mukherji, D.; Bartels, G.; Müser, M. Scaling Laws of Single Polymer Dynamics near Attractive Surfaces. *Phys. Rev. Lett.* **2008**, *100*, 068301.
15. Burgos, P.; Zhang, Z.; Golestanian, R.; Leggett, G. J.; Geoghegan, M. Directed Single Molecule Diffusion Triggered by Surface Energy Gradients. *ACS Nano* **2009**, *3*, 3235–3243.
16. Kastantin, M.; Langdon, B. B.; Chang, E. L.; Schwartz, D. K. Single-Molecule Resolution of Interfacial Fibrinogen Behavior: Effects of Oligomer Populations and Surface Chemistry. *J. Am. Chem. Soc.* **2011**, *133*, 4975–4983.
17. Yu, C.; Guan, J.; Chen, K.; Bae, S. C.; Granick, S. Single-Molecule Observation of Long Jumps in Polymer Adsorption. *ACS Nano* **2013**, *7*, 9735–9742.
18. De Gennes, P.-G. *Scaling Concepts in Polymer Physics*; Cornell University Press: Ithaca, NY, 1979.
19. Rubinstein, M.; Colby, R. *Polymers Physics*; Oxford University Press: Oxford, U.K., 2003.
20. Meyer, E. E.; Rosenberg, K. J.; Israelachvili, J. Recent Progress in Understanding Hydrophobic Interactions. *Proc. Natl. Acad. Sci. U.S.A.* **2006**, *103*, 15739–15746.

21. Skaug, M. J.; Mabry, J. N.; Schwartz, D. K. Single-Molecule Tracking of Polymer Surface Diffusion. *J. Am. Chem. Soc.* **2014**, *136*, 1327–1332.
22. Skaug, M. J.; Mabry, J.; Schwartz, D. K. Intermittent Molecular Hopping at the Solid-Liquid Interface. *Phys. Rev. Lett.* **2013**, *110*, 256101.
23. Schunack, M.; Linderoth, T.; Rosei, F.; Lægsgaard, E.; Stensgaard, I.; Besenbacher, F. Long Jumps in the Surface Diffusion of Large Molecules. *Phys. Rev. Lett.* **2002**, *88*, 156102.
24. Khatua, S.; Guerrero, J. M.; Claytor, K.; Vives, G.; Kolomeisky, A. B.; Tour, J. M.; Link, S. Micrometer-Scale Translation and Monitoring of Individual Nanocars on Glass. *ACS Nano* **2009**, *3*, 351–356.
25. Chu, P. L. E.; Wang, L. Y.; Khatua, S.; Kolomeisky, A. B.; Link, S.; Tour, J. M. Synthesis and Single-Molecule Imaging of Highly Mobile Adamantane-Wheeled Nanocars. *ACS Nano* **2013**, *7*, 35–41.
26. Bychuk, O.; O'Shaughnessy, B. Anomalous Diffusion at Liquid Surfaces. *Phys. Rev. Lett.* **1995**, *74*, 1795–1798.
27. Klafter, J.; Sokolov, I. M. *First Steps in Random Walks: from Tools to Applications*; Oxford University Press: Oxford, U.K., 2011.
28. Bénichou, O.; Loverdo, C.; Moreau, M.; Voituriez, R. Intermittent Search Strategies. *Rev. Mod. Phys.* **2011**, *83*, 81–129.
29. Bychuk, O. V.; O'Shaughnessy, B. Anomalous Surface Diffusion: A Numerical Study. *J. Chem. Phys.* **1994**, *101*, 772–780.
30. Walder, R.; Nelson, N.; Schwartz, D. K. Single Molecule Observations of Desorption-Mediated Diffusion at the Solid-Liquid Interface. *Phys. Rev. Lett.* **2011**, *107*, 156102.
31. Wong, J. S. S.; Hong, L.; Bae, S. C.; Granick, S. Polymer Surface Diffusion in the Dilute Limit. *Macromolecules* **2011**, *44*, 3073–3076.
32. Vieu, C.; Carcenac, F.; Pepin, A.; Chen, Y.; Mejias, M.; Lebib, A.; Manin-Ferlazzo, L.; Couraud, L.; Launois, H. Electron Beam Lithography: Resolution Limits and Applications. *Appl. Surf. Sci.* **2000**, *164*, 111–117.
33. Driscoll, M. K.; Sun, X. Y.; Guven, C.; Fourkas, J. T.; Losert, W. Cellular Contact Guidance through Dynamic Sensing of Nanotopography. *ACS Nano* **2014**, *8*, 3546–3555.
34. Park, M.; Harrison, C.; Chaikin, P. M.; Register, R. A.; Adamson, D. H. Block Copolymer Lithography: Periodic Arrays of ~1011 Holes in 1 Square Centimeter. *Science* **1997**, *276*, 1401–1404.
35. Bates, F. S.; Fredrickson, G. H. Block Copolymer Thermodynamics: Theory and Experiment. *Annu. Rev. Phys. Chem.* **1990**, *41*, 525–557.
36. Stoykovich, M. P.; Nealey, P. F. Block Copolymers and Conventional Lithography. *Mater. Today* **2006**, *9*, 20–29.
37. Park, C.; Yoon, J.; Thomas, E. L. Enabling Nanotechnology with Self Assembled Block Copolymer Patterns. *Polymer* **2003**, *44*, 6725–6760.
38. Hawker, C. J.; Russell, T. P. Block Copolymer Lithography: Merging "Bottom-Up" with "Top-Down" Processes. *MRS Bull.* **2005**, *30*, 952–966.
39. Segalman, R. A. Patterning with Block Copolymer Thin Films. *Mater. Sci. Eng. R* **2005**, *48*, 191–226.
40. Huang, E.; Rockford, L.; Russell, T.; Hawker, C. Nanodomain Control in Copolymer Thin Films. *Nature* **1998**, *395*, 757–758.
41. In, I.; La, Y.-H.; Park, S.-M.; Nealey, P. F.; Gopalan, P. Side-Chain-Grafted Random Copolymer Brushes as qNeutral Surfaces for Controlling the Orientation of Block Copolymer Microdomains in Thin Films. *Langmuir* **2006**, *22*, 7855–7860.
42. Campbell, I. P.; He, C.; Stoykovich, M. P. Topologically Distinct Lamellar Block Copolymer Morphologies Formed by Solvent and Thermal Annealing. *ACS Macro Lett.* **2013**, *2*, 918–923.
43. Kienberger, F.; Pastushenko, V. P.; Kada, G.; Gruber, H. J.; Riener, C.; Schindler, H.; Hinterdorfer, P. Static and Dynamical Properties of Single Poly(ethylene glycol) Molecules Investigated by Force Spectroscopy. *Single Mol.* **2000**, *1*, 123–128.
44. Park, S.; Kim, B.; Wang, J. Y.; Russell, T. P. Fabrication of Highly Ordered Silicon Oxide Dots and Stripes from Block Copolymer Thin Films. *Adv. Mater.* **2008**, *20*, 681–685.
45. Walder, R.; Kastantin, M.; Schwartz, D. K. High Throughput Single Molecule Tracking for Analysis of Rare Populations and Events. *Analyst* **2012**, *137*, 2987–2996.
46. Wang, D.; Hu, R.; Skaug, M. J.; Schwartz, D. K. Temporally Anticorrelated Motion of Nanoparticles at a Liquid Interface. *J. Phys. Chem. Lett.* **2014**, *6*, 54–59.
47. Casuso, I.; Khao, J.; Chami, M.; Paul-Gilloteaux, P.; Husain, M.; Duneau, J. P.; Stahlberg, H.; Sturgis, J. N.; Scheuring, S. Characterization of the Motion of Membrane Proteins Using High-Speed Atomic Force Microscopy. *Nat. Nanotechnol.* **2012**, *7*, 525–529.
48. Chen, Q.; Smith, J. M.; Park, J.; Kim, K.; Ho, D.; Rasool, H. I.; Zettl, A.; Alivisatos, A. P. 3D Motion of DNA-Au Nanoconjugates in Graphene Liquid Cell Electron Microscopy. *Nano Lett.* **2013**, *13*, 4556–4561.
49. Proetto, M. T.; Rush, A. M.; Chien, M. P.; Baeza, P. A.; Patterson, J. P.; Thompson, M. P.; Olson, N. H.; Moore, C. E.; Rheingold, A. L.; Andolina, C.; et al. C. Dynamics of Soft Nanomaterials Captured by Transmission Electron Microscopy in Liquid Water. *J. Am. Chem. Soc.* **2014**, *136*, 1162–1165.
50. Lu, J. Y.; Aabdin, Z.; Loh, N. D.; Bhattacharya, D.; Mirsaidov, U. Nanoparticle Dynamics in a Nanodroplet. *Nano Lett.* **2014**, *14*, 2111–2115.
51. Chechkin, A. V.; Zaid, I. M.; Lomholt, M. A.; Sokolov, I. M.; Metzler, R. Bulk-Mediated Diffusion on a Planar Surface: Full Solution. *Phys. Rev. E* **2012**, *86*, 041101.
52. Raccis, R.; Nikoubashman, A.; Retsch, M.; Jonas, U.; Koynov, K.; Butt, H.-J. r.; Likos, C. N.; Fytas, G. Confined Diffusion in Periodic Porous Nanostructures. *ACS Nano* **2011**, *5*, 4607–4616.
53. He, K.; Khorasani, F. B.; Retterer, S. T.; Thomas, D. K.; Conrad, J. C.; Krishnamoorti, R. Diffusive Dynamics of Nanoparticles in Arrays of Nanoposts. *ACS Nano* **2013**, *7*, 5122–5130.
54. Kim, T. S.; Dauskardt, R. H. Molecular Mobility Under Nanometer Scale Confinement. *Nano Lett.* **2010**, *10*, 1955–1959.
55. Metzler, R.; Jeon, J. H.; Cherstvy, A. G.; Barkai, E. Anomalous Diffusion Models and Their Properties: Non-Stationarity, Non-Ergodicity, and Ageing at the Centenary of Single Particle Tracking. *Phys. Chem. Chem. Phys.* **2014**, *16*, 24128–24164.
56. Szymanski, J.; Weiss, M. Elucidating the Origin of Anomalous Diffusion in Crowded Fluids. *Phys. Rev. Lett.* **2009**, *103*, 038102.
57. Lee, C. H.; Crosby, A. J.; Emrick, T.; Hayward, R. C. Characterization of Heterogeneous Polyacrylamide Hydrogels by Tracking of Single Quantum Dots. *Macromolecules* **2014**, *47*, 741–749.
58. Bychuk, O. V.; O'Shaughnessy, B. Anomalous Diffusion of Surface-Active Species at Liquid-Fluid and Liquid-Solid Interfaces. *J. Phys. II* **1994**, *4*, 1135–1156.